



Record bandwidth waveband-shift-free optical phase conjugation in nonlinear fiber optical loop mirror

VLADIMIR GORDIENKO,*  SONIA BOSCOLO,  MARIIA BASTAMOVA, ANDREW D. ELLIS,  AND NICK J. DORAN

Aston Institute of Photonic Technologies, Aston University, Birmingham B4 7ET, United Kingdom

*v.gordienko1@aston.ac.uk

Abstract: We present a novel configuration for broadband, wavelength-shift-free optical phase conjugation (OPC) utilizing four-wave mixing in a nonlinear fiber optical loop mirror (NOLM). In the proposed configuration, the input signals and the pump wave return to the input port of the NOLM whereas the phase-conjugated signals generated in the NOLM loop are transmitted through the output port. This allows the phase-conjugated copies to occupy the same wavelength band as the input signals, in line with the requirements for practical deployment of OPC in communication links. The demultiplexing of the phase conjugates from the input signals sharing the same band is achieved by imparting an asymmetric phase shift on the pump via a fiber Bragg grating. We experimentally demonstrate waveband-shift-free OPC with an extinction ratio between signals and conjugated copies at the NOLM output of 17 dB to 25 dB across a band of 35 nm. Whilst a 7-nm wide performance gap exists in the middle of the band, this is the record bandwidth for waveband-shift-free OPC in an all-fiber setup. We compare the experimental results with numerical simulations of the OPC-NOLM, identify the reason for the observed performance gap, and justify the route for further performance improvement.

Published by Optica Publishing Group under the terms of the [Creative Commons Attribution 4.0 License](https://creativecommons.org/licenses/by/4.0/). Further distribution of this work must maintain attribution to the author(s) and the published article's title, journal citation, and DOI.

1. Introduction

Optical phase conjugation (OPC) and other parametric devices are researched actively because of their potential for boosting the capability of optical communication systems beyond their current limits. The employment of OPC devices in communication links enables mitigation of the spectral and temporal signal distortions caused by chromatic dispersion and Kerr nonlinearity in the transmission fiber through mid-span spectral inversion, thereby improving the signal-to-noise ratio (SNR), and hence the transmission reach and capacity [1–3]. State-of-the-art OPC in multi-span links with wavelength-division multiplexed (WDM) signals has been demonstrated to outperform digital backpropagation [4], enhance the transmission reach by up to 72% [5] or 40% [6], or bring about an increasing Q -factor benefit as more OPC devices are added into the link [7,8]. Numerical simulations have also shown that the employment of an OPC-based pre-compensation module in unrepeated links can improve the SNR by up to 4 dB [9].

One of key challenges for OPC schemes is that practical optical communication links in most cases require generation of the phase-conjugated signals in the same wavelength band as the original signals and without wavelength offset, which is referred to as waveband-shift-free OPC [10]. However, the spectral inversion process is inherently transparent to the input signals, thereby leading to crosstalk between the signals and their phase conjugates unless additional measures are taken. A similar challenge is also faced by wavelength conversion optical parametric devices when the wavelength converted signals occupy the same band as the original signals [11,12]. State-of-art waveband-shift-free OPC schemes perform spectral inversion separately for each

signal half-band [4,13] or polarization [10]. These approaches either introduce upfront band splitter loss, which increases the OPC noise figure, or double the component count. Moreover, although waveband shift-free OPC across the full C and L bands has been demonstrated in periodically poled lithium niobate (when using separate phase conjugators for each signal half band) [13], the maximum bandwidth of waveband-shift-free OPC in optical fiber has been limited to about 9 nm (when splitting the signals into half-bands) [5] or about 3 nm (when splitting the signals into two polarization components) [10].

Previous works [14–17] indicate that phase-conjugated wave generation within a nonlinear Sagnac interferometer, also known as the nonlinear optical loop mirror (NOLM) [18], may enable waveband-shift-free OPC with a single pump source or a single pair of orthogonally polarized pumps for polarization insensitiveness, a single nonlinear optical medium and less upfront loss than the currently used approaches. In [14], it was demonstrated that introducing a relative phase difference between two counterpropagating four-wave mixing (FWM) waves generated in a NOLM enables inherent separation of the FWM product from both the input signal and pump waves without optical filtering. In this scheme, named the parametric optical loop mirror, the required phase difference was induced by a dispersive element asymmetrically placed in the loop. The same scheme but a second-order nonlinear optical medium was used in the theoretical study of [15]. Furthermore, by using nondegenerate pump waves in the parametric loop mirror configuration [16] or feeding two pump waves into different ports of a dispersion symmetric NOLM [17], spectral inversion with no wavelength shift was also realized. However, as the phase difference caused by chromatic dispersion depends quadratically on the frequency detuning of the signal from the pump, the parametric NOLM scheme of [14–16] works well only on a per wavelength channel basis. The scheme presented in [17] requires an additional filter to separate the phase-conjugated wave from the second pump. Alternatively, as shown by our design of an interferometric fiber-optical parametric amplifier [19], the phase-conjugated signals could be demultiplexed from the signals and pump across a wide wavelength range by shifting the pump phase in one arm of the interferometer.

In our recent proof-of-concept experiment [20], we reported on the first demonstration of multi-channel compatible waveband-shift-free OPC in a NOLM by using a fiber Bragg grating (FBG) based phase shifter asymmetrically placed in the NOLM loop to create the required phase difference between the counterpropagating phase-conjugated signals through the phase shift imparted to the degenerate pump wave. This scheme naturally separated the phase-conjugated copies generated at the signal wavelengths from both the original signals and input pump. But the relative suppression of signals against phase conjugates was around 7 dB, insufficient for practical use, and the operational wavelength band was limited to 16 nm.

This paper improves on [20] by demonstrating experimentally waveband shift-free OPC with an extinction ratio between phase conjugates and signals in the range 17 dB to 25 dB across a bandwidth of 35 nm and extends [21] with numerical simulations to provide further insight into the device operating principles. The experimental results were achieved by improving the dispersion symmetry around the gain medium in the NOLM loop and finely adjusting the asymmetric pump phase shift and in-loop polarization [22–24]. Although a side-by-side comparison with state-of-the-art demonstrations of waveband shift-free OPC in an optical fiber [5] and [10] is not possible because we performed a single-polarization demonstration and did not employ actual data signals, we demonstrate a waveband-shift-free OPC across the record wide band, which is at least three times broader than that of [5] and [10]. Therefore, this is an important proof-of-concept experiment demonstrating a fiber NOLM capability to achieve waveband shift-free OPC or, more broadly, to demultiplex unwanted FWM products and broadband WDM signals across a whole telecommunication band while using a single highly nonlinear fiber (HNLF) as the gain medium.

2. Methods

2.1. Experimental setup

The experimental setup of the waveband-shift-free OPC system is schematically depicted in Fig. 1. The pump wave (P) was sourced from a 100-kHz linewidth external cavity laser and its carrier wavelength λ_p was adjusted in the range between 1548.6 nm and 1550.0 nm during the experiment. The pump was amplified by an erbium-doped fiber amplifier (EDFA) with the output power 38.5 dBm (7.1 W), and then filtered and combined with the signals (S) via a pair of circulators and a tunable FBG centered at the pump wavelength. The signals were emulated by a WDM probe comprising 22×10 -GHz wide, 200-GHz spaced channels between 1532.7 nm and 1566.3 nm, shaped from amplified spontaneous emission (ASE) noise by a wavelength selective switch (WSS) and polarized with a polarization beam splitter (PBS). Polarization controllers (PCs) were employed within the pump and signals' paths to adjust their polarizations and align them with each other. Whilst the purpose of waveband-shift-free OPC is to allow signals and their phase conjugates (S^*) to occupy the same band at the same frequencies, for demonstration purposes, in our experiment the signals were intentionally spaced coarsely to create phase conjugates in the same band but at detuned frequencies, thereby enabling extinction ratio measurements of the phase conjugates against the signals at the OPC-NOLM output.

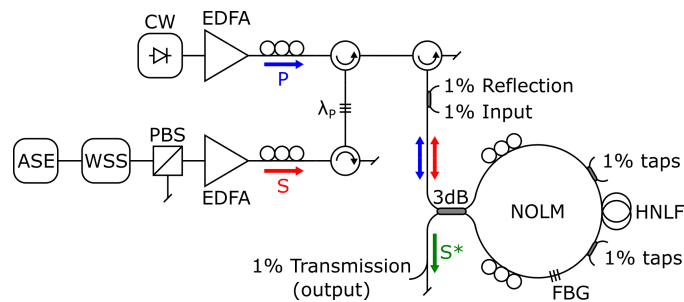


Fig. 1. Schematic diagram of the experimental setup of the waveband-shift-free OPC system. The signals (S) and pump (P) are reflected to the input port, and the phase-conjugated signals (S^*) produced in the NOLM are transmitted through the output port.

The combined pump and signals were passed to the NOLM input via an optical circulator. The NOLM loop comprised a segment of Al-doped HNLF as the nonlinear medium, a FBG based phase shifter, and two PCs for better control over birefringence induced phase shifts [22–24], connected through a spectral response flattened 3-dB coupler. The HNLF length of 52 m was relatively short to allow for broadband operation. The Al-doped HNLF had a stimulated Brillouin scattering (SBS) threshold of approximately 86 W·m, the nominal nonlinear coefficient $6.9 \text{ (W}\cdot\text{km)}^{-1}$ and the zero-dispersion wavelength 1543 nm. It is noteworthy such a fiber enables an SBS-limited nonlinear phase shift of about 0.6 rad, which is approximately twice as large as that achievable in standard HNLFs [25]. Therefore, this experiment did not require further SBS mitigation, e.g., via phase modulation of the pump source.

We used several metrics to characterize the performance of our OPC-NOLM system. The internal conversion efficiency (CE), defined as the power ratio between the signals at the input to the HNLF and their phase conjugates at the HNLF output and measured along each propagation direction inside the NOLM loop, was used to characterize the underlying FWM process. The signal conjugates' recombination efficiency, defined as the ratio of the total signal conjugates' power at the HNLF output in both propagation directions to the signal conjugates' power at the NOLM output port, assessed the ability of the asymmetric NOLM to guide the signal conjugates to the output port. The net CE, defined as the power ratio between the signals at the NOLM input

port and their phase-conjugated copies at the NOLM output port, represents the key merit of an OPC device, accounting for internal CE, recombination efficiency, and the device's insertion loss. The signal (pump) transmission through the output port, namely, the ratio of the signal (pump) powers at the NOLM output and input, provided a measure of the NOLM's ability to prevent the signals (pump) from being transmitted through the output port, hence to permit the phase-conjugated signals to occupy the same band as the original signals. The ratio of the net CE to the signal transmission defined the extinction ratio (crosstalk) between conjugates and signals, which is the key merit of a wideband shift-free OPC device. Two pairs of calibrated bidirectional 1% tap couplers were employed at both ports of the NOLM and ends of the HNLF to measure these parameters.

The phase shifter was an apodised FBG with a nominal reflectivity of 99.9% across the wavelength band 1547.1 ± 0.5 nm, which acted as a Hilbert transformer [26–28] by inducing a phase shift ϕ of up to $\pm\pi/2$ radians within several nanometers around its central wavelength. The FBG central wavelength was chosen near the center of the C band to perform waveband-shift-free OPC across the C band (considering that the OPC operation range is centered on the pump wavelength, which was adjusted around the FBG as discussed in Section 2.2). Figure 2(a) shows the measured power transmission spectrum $T(\lambda)$ of the FBG and the minimal induced phase shift, which was extracted from the spectrum by applying the Hilbert transform to $\ln\sqrt{T(\lambda)}$ [29]. Since the sensitivity of the high-resolution optical spectrum analyzer used was not sufficient to measure transmissivity values below -20 dB, we also plotted in Fig. 2(a) the calculated phase shift induced by an ideal FBG with parameters as of specification (see Sec. 2.2). Figure 2(b) is a close-up view of the wavelength range around the FBG reflection band.

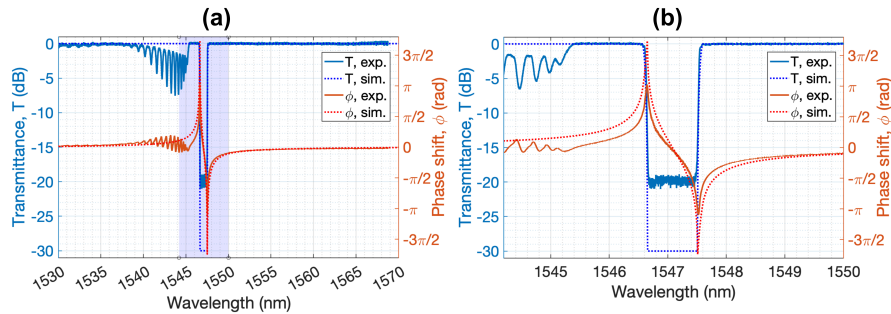


Fig. 2. (a) Transmittance and phase shift of the FBG-based phase shifter used in the experiment (solid lines) and the modelled phase shifter (dotted lines). (b) Magnified version of the shaded region in (a).

2.2. Operating principle

A perfectly symmetric loop functions as a loop mirror for the pump, the signal waves, and the signal conjugates, so all these waves always return to the original input ('reflection') port and never go through the output ('transmission') port [30]. Conversely, in an asymmetric loop where the phase shift before the HNLF in the two directions differs by $\phi(\lambda)$, while the pump and signals acquire the same total phase shift in both directions, hence they are still reflected from the loop, the selection of the output port for the signal conjugates depends on the phase difference between the counterpropagating signal conjugates as follows. The phase-conjugated optical field E_i at the output of HNLF being proportional to $E_p^2 E_s^*$ [31], where E_p and E_s are the optical fields of the pump and input signals, respectively, the conjugates in one direction inherit a phase shift of $2\phi(\lambda_p) - \phi(\lambda_s)$ from the pump and signals, while the conjugates in the opposite direction experience a phase shift of $\phi(\lambda_i)$. Therefore, the counterpropagating signal conjugates

interfere at the coupler with a total phase difference of $2\phi(\lambda_p) - \phi(\lambda_s) - \phi(\lambda_i)$. This indicates that if $\phi(\lambda_s) + \phi(\lambda_i)$ can be neglected, a pump phase shift of $\phi(\lambda_p) = (2n + 1)\pi/2$ (n an integer) enables the recombination of all conjugated signals at the NOLM output port, meaning that they are completely separated from the pump and input signals. The condition $\phi(\lambda_s) + \phi(\lambda_i) = 0$ is satisfied for a perfect dispersion symmetry inside the loop and exactly opposite phase shifts imparted by the FBG to the signals and their conjugates. However, in practice, there are always a dispersion asymmetry between the two arms of the interferometer and an asymmetry of the signals and their conjugates with respect to the center wavelength of the FBG, as well as FBG imperfections, all of which introduce asymmetric wavelength-dependent phase shifts affecting all the waves. Consequently, the signal conjugates' recombination efficiency at the NOLM output port is wavelength dependent, and the optimum pump phase shift may differ from $(2n + 1)\pi/2$. Moreover, an asymmetry in the loop birefringence also creates additional phase biases [22], which degrade the transmission/rejection of the waves through/from the desired NOLM port.

Therefore, we have done three things to achieve efficient rejection of the pump and signals from and efficient transmission of the signal conjugates through the NOLM output port. First, we employed a PC on each side of the HNLF within the NOLM loop to achieve a better control over birefringence biases than that with a single PC, and we carefully adjusted both PCs to minimize the transmission of the pump and input signals through the output port while maximizing the signal conjugates' transmission. Second, to minimize the dispersion asymmetry of the fiber loop, we equalized the optical path lengths on both sides of the HNLF with an accuracy of several centimeters by adding a length of standard single-mode fiber (SMF) to one arm. Third, we adjusted the pump wavelength around the FBG to optimize the phase shift imparted to the pump by the FBG.

2.3. Numerical model

The numerical model of the OPC-NOLM system was implemented in Matlab. The complex field envelope of the pump wave was expressed as $A_p(t) = \sqrt{P_p}e^{i\delta\phi(t)}$, where P_p is the pump power and $\delta\phi(t)$ represents the phase fluctuation induced by the non-zero spectral width of the laser source, which was modelled as a Wiener process with increments obeying a Gaussian probability distribution [32]. The pump was combined with ASE noise from an amplifier and an optical bandpass filter was used to suppress the out-of-band noise around it. Then the pump wave, polarized at 45° angle with respect to the x or y axis, was combined with co-polarized continuous-wave signals and sent to the input of a NOLM.

The input field of complex amplitude $A_{0,n}$ ($n = x, y$) was divided equally into two counterpropagating parts by a lossless and wavelength-independent 3-dB coupler, such that the amplitudes of the clockwise and counterclockwise propagating fields were given by $A_{c,n} = \sqrt{\rho_n}A_{0,n}$ and $A_{cc,n} = i\sqrt{1 - \rho_n}A_{0,n}$, respectively, where $\rho_n = 0.5$ is the field intensity coupling for the x and y polarizations. The transmitted and reflected fields at the NOLM output were obtained by using the transfer matrix of the coupler as $A_{t,n} = \sqrt{\rho_n}A'_{c,n} + i\sqrt{1 - \rho_n}A'_{cc,n}$ and $A_{r,n} = i\sqrt{1 - \rho_n}A'_{c,n} + \sqrt{\rho_n}A'_{cc,n}$, respectively, where $A'_{c,n}$ and $A'_{cc,n}$ are the two fields reaching the coupler after one round trip inside the NOLM. The NOLM loop comprised a PC, a HNLF segment, and a phase-shifting element, likewise with the setup used in the experiment. A segment δL of SMF was also included at one end of the loop to account for a residual dispersion imbalance due to non-perfect equality of the path lengths in the two arms.

We considered a PC comprising a quarter-wave plate (QWP) followed by a half-wave plate (HWP) and another QWP rotated synchronously with the first QWP, which is known to enable endless polarization transformations between any two arbitrarily varying input and output polarization states [33]. Hence, the overall transfer matrix of the cascade is given by $\mathbf{T}_c = \mathbf{Q}(\alpha + \varepsilon) \cdot \mathbf{H}(\gamma) \cdot \mathbf{Q}(\alpha)$ for the clockwise propagating field and $\mathbf{T}_{cc} = \mathbf{Q}(-\alpha) \cdot \mathbf{H}(-\gamma) \cdot \mathbf{Q}(-\alpha - \varepsilon)$ for

the counterclockwise field, where $\mathbf{Q}(\alpha)$ and $\mathbf{H}(\gamma)$ are the matrices describing the transformations of a QWP oriented at an azimuth $\alpha/2$ and a HWP oriented at an azimuth $\gamma/2$, respectively.

The field propagation in the fiber sections was modelled by two incoherently coupled nonlinear Schrödinger equations (Manakov system) for the slowly varying amplitudes of the polarization components [34], which were solved with a symmetrized split-step Fourier propagation algorithm. The HNLF had the same parameters as those of the experimental setup, but its nonlinear coefficient was adjusted slightly from the nominal value to match the experimentally observed FWM conversion efficiency. The birefringence of the fiber was assumed to be deterministic. It was modelled with a fixed strength (half of the difference between propagation constants along the x and y axes) $b = (\beta_x(\omega_p) - \beta_y(\omega_p))/2 = \pi/L_b$ and group delay per unit length $b' = b/\omega_p$ [35], where ω_p is the pump frequency, and $L_b = 26$ m is the fiber beat length, set to a value within the typical range of telecommunication fibers [36]. The SMF had a zero-dispersion wavelength of 1310 nm and a dispersion slope of 0.07ps/(nm² · km), and polarisation effects in the fiber were neglected.

The FBG-based phase shifter was modelled as an optical band-stop filter of 1-nm bandwidth, providing the complex spectral frequency response $H(\omega) = \sqrt{T(\omega)}e^{i\phi(\omega)}$, where the transmittance was the transfer function of an inverted raised cosine filter, $T(\omega) = 1 - \eta f_{RC}(\omega - \omega_f; a)$, centered at $\lambda_f = 1547.1$ nm, and with the roll-off factor $a = 0.05$ and reflection coefficient $\eta = 0.999$, and the phase $\phi(\omega)$ was calculated from the transmittance according to [29]. The transmittance and phase curves of the simulated filter are shown in Fig. 2.

3. Results and discussion

As mentioned in Sec. 2.2, we matched the optical path lengths in the NOLM on both sides of the HNLF and adjusted the pump phase shift by tuning the pump wavelength near the FBG. Figure 3 shows the measured recombination efficiency of the phase-conjugated signals (as defined in Section 2.1) as the pump wavelength was varied between 1548.6 nm and 1550.0 nm. We can see that pump wavelengths near 1550.0 nm enable a signal conjugates' recombination efficiency above -5 dB across the 35-nm spectral range being studied, excluding a several nanometers wide gap in the middle of the band. The peak transmission was limited to about -3 dB by a combination of insertion loss and a slight directional asymmetry in conversion efficiency (as described further below), resulting in unequal signal conjugates' powers in the two propagation directions inside the loop. We note that the FBG-induced phase shifts at the optimum pump wavelengths near 1550 nm are smaller than $\pi/2$ radians (Fig. 2(b)). This is due to a residual dispersion asymmetry of the fiber loop, estimated to correspond to around 5-cm path length mismatch, as shown further below.

Figure 3 also highlights that the width of the low recombination efficiency region in the middle of the spectral range scales with the pump wavelength detuning from the FBG central wavelength. This happens because of the phase shifts imparted to the signals and their conjugates by the FBG. In the case of large wavelength offsets of the signals and conjugates from the FBG, these phase shifts are small so the effect of their summation $\phi(\lambda_s) + \phi(\lambda_i)$ is negligible. Conversely, where a signal or its conjugate has a wavelength near the FBG reflection band, their phase shifts may be comparable to or even larger than the pump phase shift. This is not an issue if the signal and its conjugate are symmetric around the FBG as their phase shifts are about opposite and, thus, cancel each other out. However, the asymmetry of the signals and their conjugates around the FBG increases as the pump is detuned from the FBG central wavelength, which, in turn, increases the range where $\phi(\lambda_s) + \phi(\lambda_i)$ is sufficiently large to lessen the conjugate's recombination at the NOLM output port.

Based on the results of Fig. 3 altogether, we chose the pump wavelength of 1549.72 nm because it enabled a conjugates' recombination efficiency above -7 dB across the 35-nm spectral range, while limiting the low recombination efficiency bandwidth to approximately 5 nm. Furthermore,

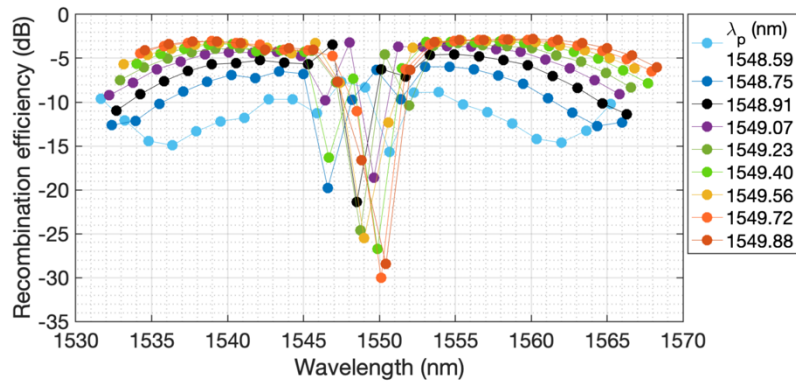


Fig. 3. Recombination efficiency of the signal conjugates at the NOLM output port as the pump wavelength is adjusted from 1548.6 nm (light blue) to 1550.0 nm (red).

as this pump wavelength corresponds to a frequency of 193.45 THz, it allowed for the signals and their conjugates to be on the standard 50-GHz frequency grid (ITU-T G.694.1).

The overall optimum results are summarized in Fig. 4(a), which shows the performance indicators defined in Section 2.1, namely, the internal and net CEs, and the signal and pump transmissions through the output port. We can see that an internal CE of -14 dB to -10 dB is achieved across the 35-nm spectral range. It was restricted by the SBS-limited pump power in each direction in the HNLF (32 dBm). There is a difference of approximately 1 dB in internal CE between the clockwise and the counterclockwise directions. This asymmetry causes some penalty for the signal conjugates' recombination efficiency. The net CE, which includes the insertion loss and the signal conjugates' recombination efficiency at the NOLM output, is in the range -18.5 dB to -14 dB, except for the two signal conjugates near the pump whose recombination was degraded by the phase shift imparted by the FBG to them and/or the corresponding input signals. The signal transmission through the output port is largely below -35 dB (i.e., less than 0.1%) across the 35-nm range. This was achieved after careful adjustment of the polarization inside the loop. The transmission of the signal at 1547 nm is high because the counterclockwise signal part was reflected by the FBG, thereby impairing the interference of the two signal parts at the NOLM output. It is unclear why the transmission of the channels at 1548 nm and 1552 nm is several decibels higher than that of other channels, but this does not represent a critical performance degradation as their transmission is still below -30 dB. Figure 4(a) also shows an excellent pump rejection from the output port at a level of -39 dB.

Figure 4(b) shows the numerically calculated performance curves obtained for the same pump wavelength used in Fig. 4(a) and each of three scenarios: i) a perfect dispersion symmetry inside the loop (achieved in the model when no SMF segment is included in the loop), and a small dispersion asymmetry induced by SMF lengths of ii) $\delta L = 5$ cm and iii) $\delta L = 10$ cm. The internal CE is around -10 dB across the whole 35-nm spectral range, in a fair agreement with the experiment. The net CE is also in a good quantitative agreement with the experiment, where both the simulated and experimental net CE curves feature the same dip in the middle of the spectral range. The small divergence between the two curves around 1546 nm and 1552 nm is due to the experimental internal CE dips at these wavelengths. We can observe from Fig. 4(b) that the effect of a small dispersion asymmetry inside the loop is to reduce the net CE at the edges of the spectral band compared with the ideal case of perfect dispersion symmetry, whilst the signal transmission through the output port is not affected, which is consistent with the theoretical predictions [14,30]. The simulated curve with an optical path asymmetry of 5 cm shows the best match with the experiment, thus providing an estimate for the optical path mismatch in the experiment. We

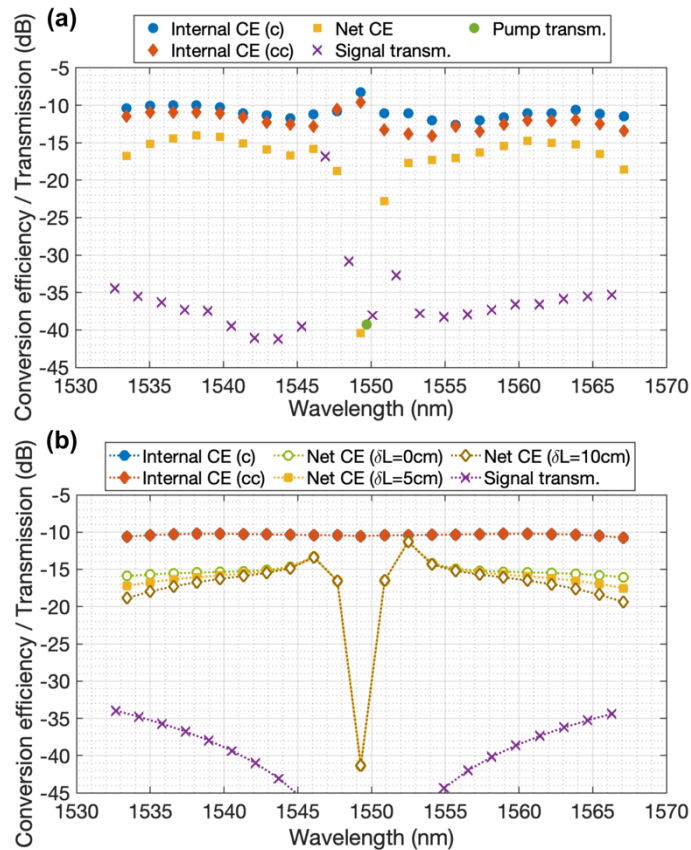


Fig. 4. (a) Experimentally measured overall optimized internal (clockwise – blue, counter-clockwise – red) and net (yellow) CEs, and signal transmission (purple). The pump transmission is also shown (green). (b) Numerically calculated internal and net CEs, and signal transmission, for the in-loop SMF lengths $\delta L = 0, 5,$ and 10 cm, and the PC settings ($\alpha = 0, \gamma = 10\pi/11, \varepsilon = \pi$).

can also see in Fig. 4(b) that the curve representing the signal transmission through the output port matches well the experimental results in Fig. 4(a) in the outer regions of the spectral range being considered. The numerical results were obtained by introducing a small amount of circular polarization ($2\pi/11$ radians) via tuning of the angular orientation γ of the HWP. It is noteworthy that for the PC settings: ($\alpha = 0, \gamma = \pi, \varepsilon = \pi$), which correspond to a constant and linear phase retardation of π radians induced by the controller [33], the numerically calculated rejection of all the signals at the output port was complete. This indicates that some fiber birefringence in the NOLM had remained uncompensated in the experiment and confirms the importance of a fine adjustment of the in-loop polarization for optimum signal and pump rejection at the NOLM output. Other potential factors contributing to the signal and pump transmission floor of around -40 dB in the experiment include Rayleigh backscattering and/or back reflections, which add incoherently in the coupler.

The extinction ratio between conjugates and signals at the NOLM output port, extracted from Fig. 4, is plotted in Fig. 5. This is a key parameter indicating the level of crosstalk at the NOLM output. It was calculated for each signal and each conjugate in relation to their two closest conjugates and signals, respectively, and the minimum (worst) value was chosen in each case. The experimental extinction ratio (obtained from Fig. 4(a)) is between 17 dB and 25 dB across

the 35-nm band except for a 7-nm wide gap in the middle. A previous work [37] has shown that crosstalk levels around 16 dB and 24 dB cause 1-dB signal-to-noise penalty at a bit-error rate of 10^{-3} for quadrature phase-shift keying (QPSK) and 16 quadrature-amplitude modulation (QAM) signals, respectively. This means that the extinction ratio demonstrated in this work is tolerable for QPSK signals but would require an improvement for 16-QAM signals. Then, it is important to note that the extinction ratio is identical to the ratio between the net CE and the signal transmission because these merits define output powers of the conjugates' and signals' powers respectively with relation to the same input signal power. Hence, the extinction ratio improvement may be achieved via increase of the internal CE in our NOLM setup, which would require further SBS threshold enhancement by strain [10], temperature gradient [38], or other means such as pump-phase modulation [5]. For example, an internal CE of around 0 dB was achieved in [10], which enabled OPC operation with 16-QAM signals at an extinction ratio of 26 dB. This indicates that a 10-dB enhancement of the internal CE in the NOLM would achieve an extinction ratio level of at least 27 dB across the claimed wavelength range, which would be sufficient for 16-QAM signals.

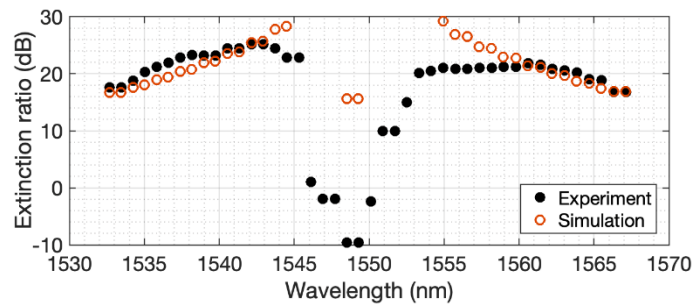


Fig. 5. Experimentally measured (black) and numerically calculated (red) extinction ratio between phase-conjugated signals and input signals at the NOLM output port.

The performance gap in the middle of the 35-band observable in Fig. 4(a) can be reduced by improving the NOLM dispersion symmetry, which would permit to set the pump wavelength closer to the FBG, and by employing a FBG with narrower reflection band. The simulated extinction ratio (obtained from Fig. 4(b) for $\delta L = 5$ cm) is in good quantitative agreement with the experimental one across the outer regions of the 35-nm spectral range, while it deviates from the experimental one, becoming significantly higher, in the central region between 1543 nm and 1560 nm where the simulated signal transmission at the NOLM output is below -40 dB.

Figure 6(a) shows the calibrated optical power spectra at the NOLM input and output relating to the optimum experimental results (Fig. 4(a)). It highlights that the input signals are almost non-existent at the output except for the signal at about 1547 nm, whose rejection is disrupted by reflection from the FBG. Consequently, the signal conjugates (new wavelengths) appearing in-between the signals have a high extinction ratio with the signals at the output. In addition, Fig. 6(a) shows that although pump is not eliminated from the output, its power of -3 dBm is sufficiently low to avoid unwanted interaction with signals during transmission. The corresponding numerically calculated power spectra for $\delta L = 5$ cm are displayed in Fig. 6(b).

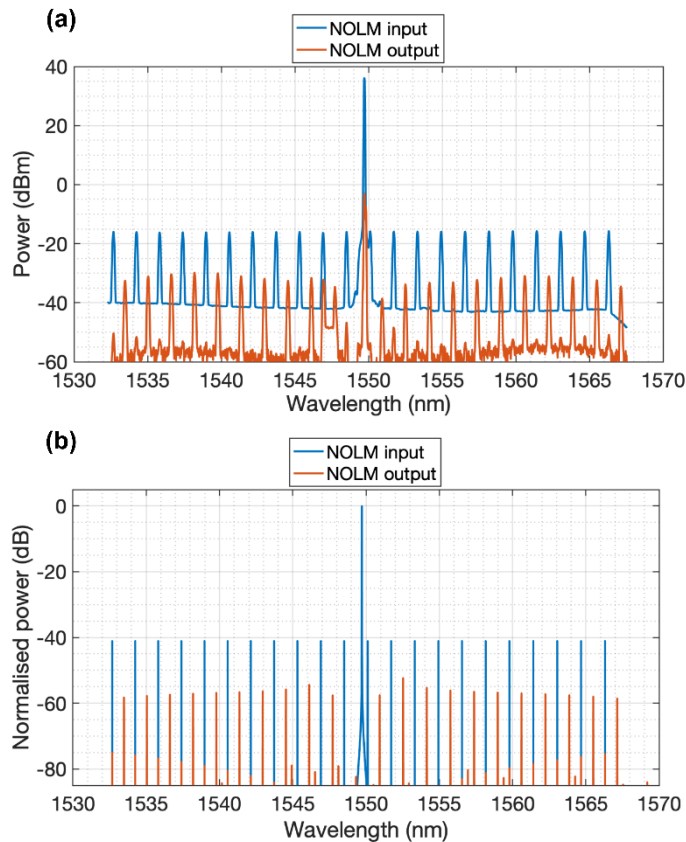


Fig. 6. (a) Experimentally measured and (b) numerically calculated optical power spectra at the NOLM input (blue) and output (red). The effective resolution bandwidth of the optical spectrum analyzer was 10 GHz, matching the probes' linewidths.

4. Conclusion

We have experimentally demonstrated that phase-conjugated wave generation within a NOLM setup is capable of broadband, waveband shift-free OPC by showing an extinction ratio between signal conjugated copies and signal 17 dB and 25 dB across a wavelength range of 35 nm except for a 7-nm gap in the middle. We have discussed the way forward for improving the extinction ratio and significantly reducing the performance gap. Numerical simulations of the OPC-NOLM model have been used to both guide and validate the experimental results. The approach, demonstrated here for single-pump OPC, can also enable polarization-independent OPC with a single pair of orthogonally polarized pumps. Overall, the work presented here represents an important proof of concept demonstrating the great potential of interferometers (NOLM or Mach-Zehnder) for broadband rejection of unwanted FWM products in optical parametric devices. Indeed, we believe this is a promising technology for waveband shift-free OPC and related parametric devices such as parametric amplifiers and wavelength converters, where it may be required to avoid crosstalk between signals and idlers or wavelength converted copies, occurring at the same wavelengths.

Funding. Engineering and Physical Sciences Research Council (EP/R024057/1, EP/S003436/1, EP/S016171/1, EP/X019241/1, EP/X031918/1).

Disclosures. The authors declare no conflicts of interest.

Data availability. Data underlying the results presented in this paper are available in Ref. [39].

References

1. S. Watanabe, S. Kaneko, and T. Chikama, "Long-haul fiber transmission using optical phase conjugation," *Opt. Fiber Technol.* **2**(2), 169–178 (1996).
2. A. D. Ellis, M. E. McCarthy, M. A. Z. Al Khateeb, *et al.*, "Performance limits in optical communications due to fiber nonlinearity," *Adv. Opt. Photonics* **9**(3), 429–503 (2017).
3. A. D. Ellis, M. C. Tatham, D. A. O. Davies, *et al.*, "40 Gbit/s transmission over 202 km of standard fibre using mid span spectral inversion," *Electron. Lett.* **31**(4), 299–301 (1995).
4. I. Sackey, F. Da Ros, T. Richter, *et al.*, "Kerr nonlinearity mitigation: Mid-link spectral inversion versus digital backpropagation in 5×28-GBd PDM 16-QAM signal transmission," *J. Lightwave Technol.* **33**(9), 1821–1827 (2015).
5. M. A. Z. Al-Khateeb, M. Tan, M. A. Iqbal, *et al.*, "Experimental demonstration of 72% reach enhancement of 3.6Tbps optical transmission system using mid-link optical phase conjugation," *Opt. Express* **26**(18), 23960–23968 (2018).
6. T. Umeki, T. Kazama, A. Sano, *et al.*, "Simultaneous nonlinearity mitigation in 92 × 180-Gbit/s PDM-16QAM transmission over 3840 km using PPLN-based guard-band-less optical phase conjugation," *Opt. Express* **24**(15), 16945–16951 (2016).
7. M. E. McCarthy, M. A. Z. Al-Khateeb, and A. D. Ellis, "PMD tolerant nonlinear compensation using in-line phase conjugation," *Opt. Express* **24**(4), 3385–3392 (2016).
8. H. Hu, R. M. Jopson, A. H. Gnauck, *et al.*, "Fiber nonlinearity mitigation of WDM-PDM QPSK/16-QAM signals using fiber-optic parametric amplifiers based multiple optical phase conjugations," *Opt. Express* **25**(3), 1618–1628 (2017).
9. P. M. Kaminski, T. Sutli, J. H. C. Júnior, *et al.*, "All-optical nonlinear pre-compensation of long-reach unrepeated systems," in *46th European Conference on Optical Communications (ECOC 2020)*, paper Tu1F.1.
10. I. Sackey, C. Schmidt-Langhorst, R. Elschner, *et al.*, "Waveband-shift-free optical phase conjugator for spectrally efficient fiber nonlinearity mitigation," *J. Lightwave Technol.* **36**(6), 1309–1317 (2018).
11. T. Kato, S. Watanabe, T. Tanimura, *et al.*, "THz-range optical frequency shifter for dual polarization WDM signals using frequency conversion in fiber," *J. Lightwave Technol.* **35**(6), 1267–1273 (2017).
12. A. Sobhanan, V. Gordienko, C. B. Gaur, *et al.*, "All-optical any-to-any wavelength conversion across 36 nm range," in *48th European Conference on Optical Communication (ECOC 2022)*, paper We5.4.
13. S. Shimizu, T. Kobayashi, T. Kazama, *et al.*, "Hybrid lumped repeater using PPLN-based high-gain optical parametric phase conjugators and EDFAs for C + L-band transmission," *J. Lightwave Technol.* **42**(10), 3580–3591 (2024).
14. K. Mori, T. Morioka, and M. Saruwatari, "Optical parametric loop mirror," *Opt. Lett.* **20**(12), 1424–1426 (1995).
15. Y. Okamura and A. Takada, "Waveband-shift-free optical phase conjugator based on difference-frequency generation," *Opt. Express* **28**(5), 7596–7606 (2020).
16. K. Mori, T. Morioka, and M. Saruwatari, "Wavelength-shift-free spectral inversion with an optical parametric loop mirror," *Opt. Lett.* **21**(2), 110–112 (1996).
17. H. C. Lim, F. Futami, and K. Kikuchi, "Polarization independent wavelength-shift-free optical phase conjugator using a nonlinear fiber Sagnac interferometer," *IEEE Photon. Technol. Lett.* **11**(5), 578–580 (1999).
18. N. J. Doran and D. Wood, "Nonlinear-optical loop mirror," *Opt. Lett.* **13**(1), 56–58 (1988).
19. V. Gordienko, F. M. Ferreira, V. Ribeiro, *et al.*, "Design of an interferometric fiber optic parametric amplifier for the rejection of unwanted four-wave mixing products," *Opt. Express* **31**(5), 8226–8239 (2023).
20. V. Gordienko, M. Bastamova, A. Ellis, *et al.*, "Nonlinear optical loop mirror for waveband-shift free optical phase conjugation," in *Optical Fiber Communication Conference (OFC 2023)*, paper Th2A.12.
21. V. Gordienko, S. Boscolo, M. Bastamova, *et al.*, "Waveband-shift-free optical phase conjugation in fiber loop mirror across 35-nm bandwidth," in *Optical Fiber Communication Conference (OFC 2024)*, paper M1B.4.
22. E. A. Kuzin, N. Korneev, J. W. Haus, *et al.*, "Theory of nonlinear loop mirrors with twisted low-birefringence fiber," *J. Opt. Soc. Am. B* **18**(7), 919–1060 (2001).
23. O. Pottiez, E. A. Kuzin, B. Ibarra-Escamilla, *et al.*, "Easily tunable nonlinear optical loop mirror based on polarization asymmetry," *Opt. Express* **12**(16), 3878–3887 (2004).
24. B. Ibarra-Escamilla, E. A. Kuzin, P. Zaca-Morán, *et al.*, "Experimental investigation of the nonlinear optical loop mirror with twisted fiber and birefringence bias," *Opt. Express* **13**(26), 10760–10767 (2005).
25. V. Gordienko, Á. D. Szabó, M. F. C. Stephens, *et al.*, "Limits of broadband fiber optic parametric devices due to stimulated Brillouin scattering," *Opt. Fiber Technol.* **66**, 102646 (2021).
26. M. H. Asghari and J. Azaña, "All-optical Hilbert transformer based on a single phase-shifted fiber Bragg grating: design and analysis," *Opt. Lett.* **34**(3), 334–336 (2009).
27. M. Li and J. Yao, "All-fiber temporal photonic fractional Hilbert transformer based on a directly designed fiber Bragg grating," *Opt. Lett.* **35**(2), 223–225 (2010).
28. C. Sima, J. C. Gates, M. N. Zervas, *et al.*, "Review of photonic Hilbert transformers," *Front. Optoelectron.* **6**(1), 78–88 (2013).
29. M.-C. N. Dicaire, J. Upham, I. De Leon, *et al.*, "Group delay measurement of fiber Bragg grating resonances in transmission: Fourier transform interferometry versus Hilbert transform," *J. Opt. Soc. Am. B* **31**(5), 1006–1010 (2014).
30. D. B. Mortimore, "Fiber loop reflectors," *J. Lightwave Technol.* **6**(7), 1217–1224 (1988).

31. M. E. Marhic, "Scalar OPA theory," in *Fibre Optical Parametric Amplifiers, Oscillators and Related Devices* (Cambridge University, 2008), pp. 31–77.
32. M. Lax, "Classical noise. v. noise in self-sustained oscillators," *Phys. Rev.* **160**(2), 290–307 (1967).
33. F. Heismann, "Analysis of a reset-free polarization controller for fast automatic polarization stabilization in fiber-optic transmission systems," *J. Lightwave Technol.* **12**(4), 690–699 (1994).
34. G. P. Agrawal, "Polarization effects," in *Nonlinear Fiber Optics*, 5th ed. (Academic, 2013), pp. 193–244.
35. C. R. Menyuk, "Nonlinear pulse propagation in birefringent optical fibers," *IEEE J. Quantum Electron.* **23**(2), 174–176 (1987).
36. C. R. Menyuk and B. S. Marks, "Interaction of polarization mode dispersion and nonlinearity in optical fiber transmission systems," *J. Lightwave Technol.* **24**(7), 2806–2826 (2006).
37. P. J. Winzer, "High-spectral-efficiency optical modulation formats," *J. Lightwave Technol.* **30**(24), 3824–3835 (2012).
38. C. Guo, M. Vasilyev, Y. Akasaka, *et al.*, "Temperature-tuned two-segment highly-nonlinear fiber with increased stimulated Brillouin scattering threshold," in *Optical Fiber Communication Conference (OFC 2023)*, paper Th1B.2.
39. V. Gordienko, S. Boscolo, M. Bastamova, *et al.*, "Data underpinning article "Record bandwidth waveband-shift-free optical phase conjugation in nonlinear fiber optical loop mirror"," Aston University (2024), <https://doi.org/10.17036/researchdata.aston.ac.uk.00000643>.